Proceedings of the 5th h World Congress on Momentum, Heat and Mass Transfer (MHMT'20)
~~Lisbon, Portugal~~ Virtual Congress – October 2020
Paper No. ENFHT 166
DOI: 10.11159/enfht20.166

Investigating the influence of macroscopic surface structures on the thermal contact conductance using infrared thermography

Thorsten Helmig, Michael Burghold, Faruk Al-Sibai, Reinhold Kneer
Institute of Heat and Mass Transfer, RWTH Aachen University
Augustinerbach 6, 52062 Aachen, Germany
helmig@wsa.rwth-aachen.de

Abstract **-** The prediction of thermal contact conductance is commonly based on surface parameters such as roughness or mean slope. However, these parameters do not consider the orientation of macroscopic surface structures in contact, although this parameter may have a significant influence on the thermal contact conductance. To investigate this effect, three sets of specimens with different orientation of macroscopic surface structures are manufactured, all revealing the same roughness and mean slope. To quantify the thermal contact conductance, an infrared-camera measures the transient temperature response of two heated specimens pressed together by a hydraulic test bench. The obtained temperature data are then used as input for a conjugate gradient method quantifying the time-dependent thermal contact conductance. The results yield that specimen sets offering a conforming contact interface exhibit the highest conductance but show at the same time the highest standard deviation. In contrast, non-conforming contacts reveal both, lower mean values and standard deviation, the latter leading to less uncertainty in predicting thermal contact conductance. With the outlined findings, distinct surface structures can be chosen in order to achieve a desired range of thermal characteristics.

Keywords**:** Thermal Contact Conductance, macroscopic surface structures, IR-thermography, Inverse heat conduction problem**.**

1. Introduction

For a precise modeling of thermal systems and processes, detailed knowledge about the acting thermal boundary conditions is of major importance. In particular, the thermal characterization of machine tools requires a detailed insight into heat transfer between joint components to predict the respective thermal expansion of machine components and to allow for a more precise manufacturing process [1-2]. Due to processing, technical surfaces are never perfectly flat, but can rather be represented by a high amount of asperities. Therefore, the actual contact area equals only a fraction of the nominal area of surfaces in contact. This characteristic results in a thermal resistance, leading to constriction of heat flow and thus, to a temperature drop across the contact interface. With a given temperature difference at the interface ΔT_c and the transferred heat flux $\dot{q}''$ the resistance R_c and corresponding contact heat transfer coefficient h_c are defined as:

$$R_c = \frac{\Delta T_c}{\dot{q}''} \Leftrightarrow h_c = \frac{\dot{q}''}{\Delta T_c} \tag{1}$$

Cooper et al. [3] presented a common analytical approach to predict the thermal contact conductance in dependence of surface parameters such as roughness σ, mean slope m and surface load p. This approach has been continuously extended by Mikic [4] and Yovanovich [5], also considering effects of interstitial fluids on the thermal contact conductance [6,7]. A detailed summary of proposed approaches can be found in the work by Yovanovich [8]. Most of the derived analytical approaches use the mentioned properties (σ and m) to characterize the surface under investigation and further assume a gaussian and isotropic height distribution of the surface profile. However, this assumption may not be valid for all technically processed surfaces showing distinctive profiles as a result of the chosen manufacturing process [9-11]. Therefore, several attempts exist to parameterize surface profiles in dependence of the applied manufacturing process [12-14]. On this context, the parameters also need to consider the actual cutting direction and the resulting macroscopic surface structure. For example, in milling processes the orientation of the surface grooves coincides with the actual cutting direction of the milling tool. This might have significant influence on the thermal contact conductance and can lead to uncertainties in predicting the temperature fields in the system, in particular if components can be assembled in different directions. To quantify this effect,

three sets of specimens with different orientations of macroscopic surface structures are manufactured, however all revealing almost the same microscopic surface roughness and mean slope. Therefore, the aim of this work is to investigate whether there is a general impact of macroscopic surface structure orientation on the thermal contact conductance for surfaces with an approximately equal roughness and mean slope.

2. Experimental Methods and Surface Preparation

The experimental setup used is similar to the outlined design in Burghold et al. [15, 16] and also shown in Figure 1. The framework of this setup consists of a custom-made servo-hydraulic material testing system, providing maximum forces up to 100 kN. Specimens under investigation are placed into an upper and lower socket of the testing system each enclosed with a pair of heaters for specimen temperature regulation. The lower and upper specimen are heated to a temperature level between 45-50 °C and 95-100 °C, respectively, and are provided with small sockets for thermocouples to monitor the heating process. After pneumatic retraction of the heaters, the specimens are pressed together which is managed by an integrated PID controller. This controller regulates the applied force on the specimen pairing and allows for an overshooting of the target load before reaching steady state pressure as exemplarily shown in Figure 1. This effect has been used in previous investigations to mimic oscillating forces [15, 16]. The pressing process itself is recorded with an Infratec ImageIR 5300 infrared camera equipped with a macro lens, providing an optical resolution of 25 μm/pixel. For measurements, the front surfaces of the specimens are painted black to obtain a specified surface emissivity of $\varepsilon = 0.972$ [17] (Figure 1). While the initial recording frequency is set to 2000 Hz to track the specimens edge at the beginning of the pressing, the data is later down sampled to 250 Hz to filter high frequent oscillations in the thermal analysis. In contrast to steady state measurements with thermocouples inside the specimens, infrared thermography offers recordings of whole temperature fields at high recording frequencies. This setup further, enables transient measurements with varying pressure and significant shorter investigation times. Considering the accuracy of the experiments presented in this work, the temperature accuracy is expected to be in range of ±0.2 K and the spatial accuracy in magnitude of one pixel (25 μm/pixel).

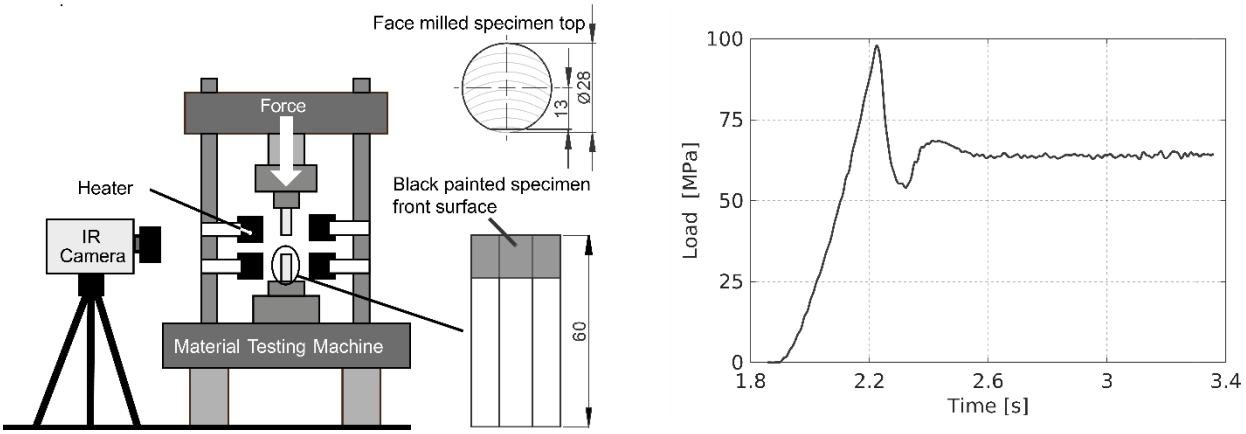

Fig. 1: Used experimental setup [15]. A close-up of the specimen geometry shows the investigated specimen front for temperature measurements. All measures are given in millimeter. Further, an exemplary load trend is shown.

For manufacturing the specimens, a C45 steel is used, which is a very common material in process and automotive engineering. Also, the material properties are representative for several other steels used in this field. The particular C45 steel used in this investigation reveals a hardness of 240 HV, 2000 MPa, a density of 7800 kg/m, a heat capacity of 420 J/kgK and a heat conductivity of 48 W/mK. The actual surfaces are manufactured by face milling with the parameters outlined in Table 1.

By varying the cutting direction and angle, different orientations of surface grooves are obtained, which is shown in the left subimages of Figure 2.

Table 1: Processing parameters for face milled contact surfaces.

Feed [mm]	Stepover [mm]	Cutting speed [m/min]
0.1	0.2	28

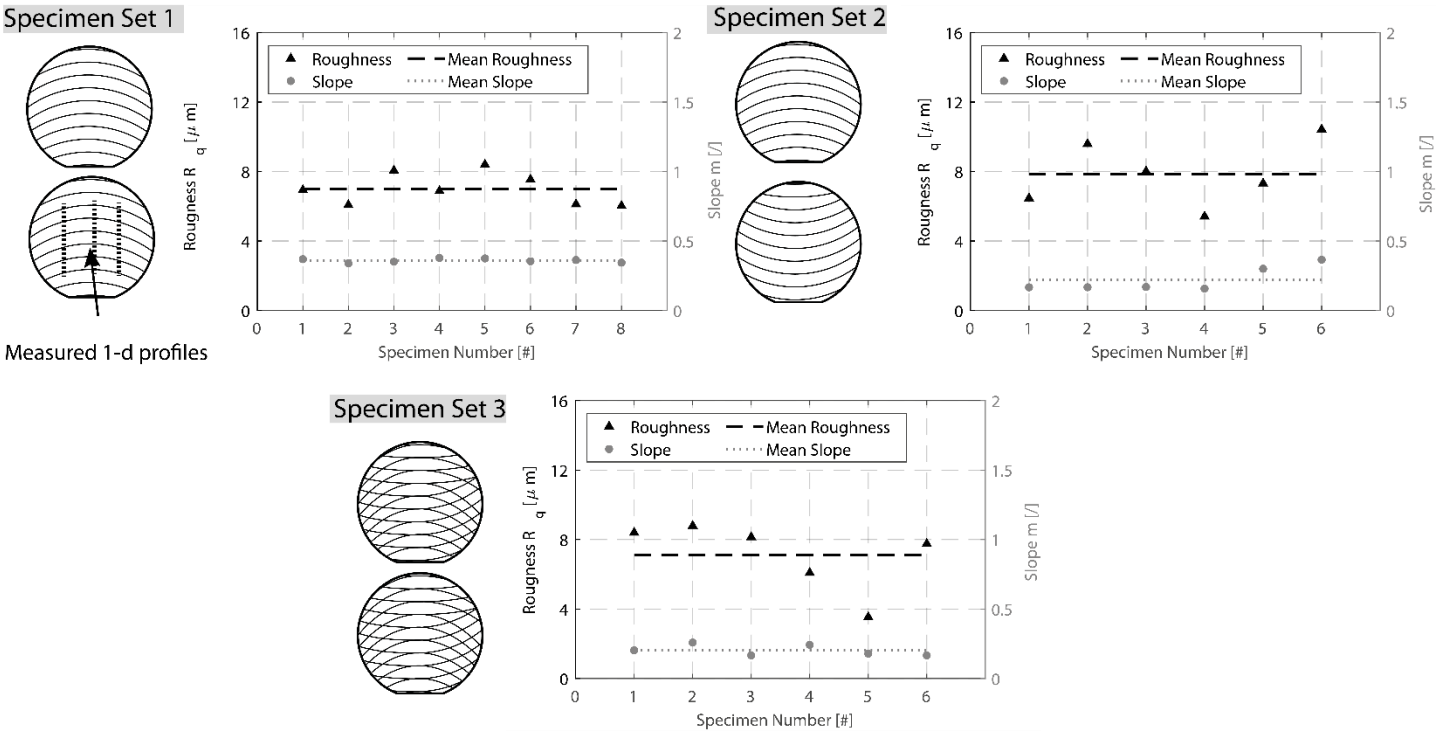

Fig. 2: Visualization of the three sets of specimens used for experimental investigation. Roughness and mean slope of each investigated specimen are shown in the adjacent plots. Data points indicate values of specific specimens, lines show the mean value.

For the first set, all specimens are manufactured with a forward cutter direction, resulting in equal orientation of surface structures for all specimens. In contrast for the second set, the specimens are manufactured with varying cutting directions. Half of the specimens are manufactured with a forward cutting direction, while the second half is processed with a backward oriented cutter. In the following experimental investigation one forward and one backward manufactured specimen are brought into contact. For the third set, the surfaces are manufactured with an angled cutter, causing a mix of the surface profile from the first and second specimen set. After processing all sets, three parallel line profiles from all specimens are measured with a tactile profilometer and are following averaged in order to determine the surface roughness and mean slope. This is visualized on the right hand-side of the subimages in Figure 2 revealing individual roughness values between 6-10 μm and a mean value of approximately 8μm. Further, the mean slope of all specimens is approximately 0.25-0.35.

Though, all specimens reveal approximately the same roughness and mean slope, the different orientation of surface grooves induces different contact scenarios. The first specimen set offers conforming as well as a non-conforming contact interface. In a non-conforming contact scenario (Figure 3a) only the peaks of the specimen surfaces get into contact causing a constriction of the heat flow at the interface and a smaller thermal contact conductance compared to conforming or semi conforming surface contact (Figure 3 b-c). Considering the second specimen set, the different orientation of structures inhibits a conforming surface contact (Figure 3 d). Hence, less total contact area and a smaller thermal contact conductance

is expected. Similar behaviour is expected for the third specimen set, where the mix of forward and backward oriented surface grooves does not allow for a microscopically conforming surface contact. However, due to the higher density of surface grooves, slightly higher values of thermal contact conductance are expected compared to the second specimen set. For each specimen pairing the experiments are repeated several times to get representative impression of statistical effects.

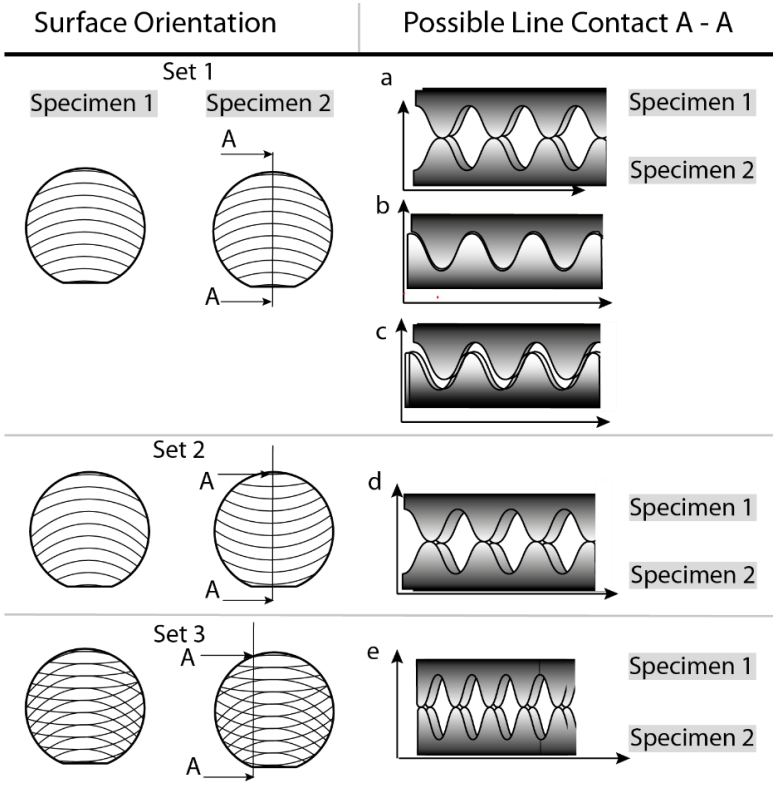

Fig. 3: Visualization of the different contact scenarios for each specimen set. The line profile A - A shows possible contact lines for each set.

3. Evaluation Algorithm

Prior to the actual thermal analysis, recorded data from measurements need to be associated to the upper and lower specimen to be able to extract their respective thermal response due to the contact.

To automate this process, intensity gradients of the recorded video data is used to locate and track the specimens' edges during the course of the experiment. Afterwards, the acting thermal boundary condition is quantified yielding an inverse heat transfer problem. This problem is characterized by knowing the effect of an acting boundary condition or thermophysical property rather than the property itself. A common approach to solve this problem is the conjugate gradient method which has been presented in many publications [15, 18-21]. Therefore, only a short summary is outlined here.

The conjugate gradient method aims for the minimization of an objective function J defined as:

$$J = \int_{t_0}^{t} T(h_c(t) - Y)^2 dt \tag{2}$$

In the case of one measurement temperature in each specimen simplifies to

$$J = \int_{t_0}^{t} (T_1 - Y_1)^2 + \ (T_2 - Y_2)^2 \, dt \tag{3}$$

Here, Y_i corresponds to the exprimental temperature data and T_i is the calculated temperature, subject to the energy equation. Due to a small Biot number of less than 0.01 a one-dimensional heat conduction with a characteristic length of 4 A/P (A Surface Area and P perimeter) can be assumed.

$$\rho c_p \frac{\partial T}{\partial t} = k \frac{\partial T^2}{\partial x^2} - h_{amb} \frac{P}{A} (T - T_{amb}) \tag{4}$$

Here, ρ, c_p and k denote the materials density, heat capacity and conductivity, respectively. Furthermore, the factor h_{amb} accounts for both convective and radiative heat losses to the environment with temperature T_{amb}.
To solve the minimization problem, an iterative procedure is applied varying the previously assumed thermal contact conductance and recalculating the corresponding T_i until a desired agreement between measurements and calculated temperature is achieved. In this case the difference between two successive objective function values ($\Delta J < 5\ 10^{-5} K^2 s$) is used as a stopping criterion.

4. Results and Discussion

Following, experimental results of the three outlined specimen sets are presented (Figure 4 - 6). Starting with the first set, a linear elastic-trend of the mean thermal contact conductance is shown, taking maximum values of 22 kW/m^2, but yielding as well a significant standard deviation, in particular at high load (Figure 4). A reason for this trend is the existence of conforming as well as non-conforming surface contacts. Depending on the actual specimen pairing, the fraction of the surface area in contact can vary considerably, leading to the outlined variations in thermal contact conductance.

As the results of performed experiments are primarily used as boundary conditions in modelling thermal systems, this variations in contact conductance cause significant uncertainties in the prediction of corresponding temperature fields.

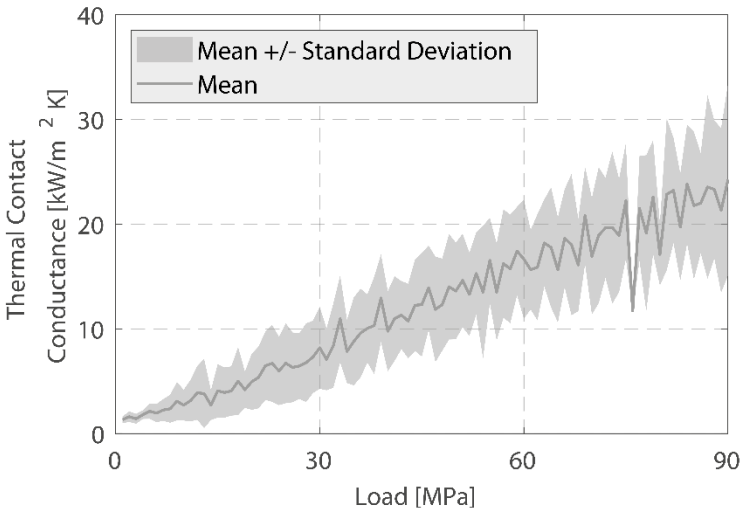

Fig. 4: Load dependent mean value and standard deviation of the thermal contact conductance for the first set of specimens.

In contrast, the second specimen set yields minor heat transfer coefficients with a more compact distribution of results with a maximum mean heat transfer coefficient 17 kW/m^{2}K. These differences arise primarily due to the non-conforming contact interface with fewer contact spots, leading to a constriction of heat flow. Regarding the slope, the linear elastic trend at the beginning quickly transitions into a logarithmic tendency at higher loads, suggesting plastic surface deformation.

Nevertheless, this set reveals a minor standard deviation compared to the first set, facilitating a more accurate estimation of thermal contact conductance and therefore less uncertainty in the predicted temperature fields.

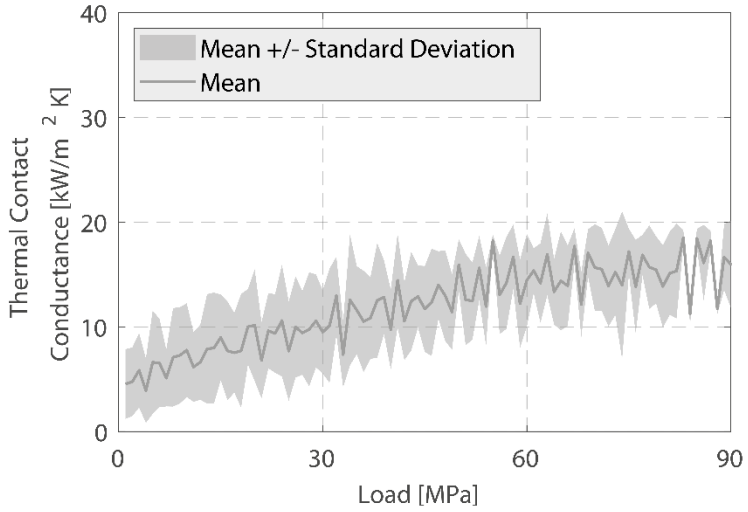

Fig. 5: Load dependent mean value and standard deviation of the thermal contact conductance for the second set of specimens.

The third investigated specimen set accounts for the mix of forward and backward cutting direction (Figure 6) and shows in general a similar trend as for the second set, since in this setup the interface is also dominated by a non-conforming contact interface. Analogous to the second set, the measurements exhibit a linear-elastic behaviour at first, which transitions then into a logarithmic inclination. Apart from higher maximal thermal contact conductances of 19 kW/m^2K, also a minor standard deviation compared to the second case is obtained. Consequently, this specimen set provides the highest degree of certainty in particular if the quantified conductance values are later used as a boundary condition for the modeling of thermal systems.

Though all experimental investigations are performed with a limited number of specimens, a clear tendency for all three sets is visible. Hence, future investigations will focus on a comprehensive analysis of different materials as well as a larger set of specimens in order to get more detailed statistics. Further, the performed experiments will be repeated with numerical models to investigate whether these are also able to exhibit the phenomena under investigation.

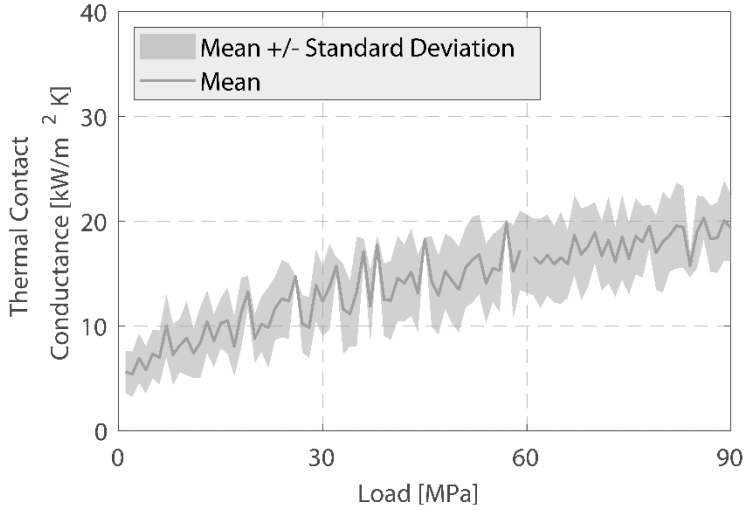

Fig. 6: Load dependent mean value and standard deviation of the thermal contact conductance for the third set of specimens.

Conclusion

In this work, the impact of macroscopic surface structure and orientation on the thermal contact conductance is presented. Basis for these investigations are three different types of face-milled specimen sets, showing all the same roughness and mean slope but are manufactured with different cutter directions. The specimen pairings are located in a servo-hydraulic material testing system, heated to two distinct temperature levels and following brought into contact. The pressing process and resulting temperature equalization are recorded by means of a high-speed IR camera. The obtained temperature data is following used to quantify the time dependent thermal contact conductance. The experimental results reveal, that the highest thermal contact conductances are obtained by specimens yielding the same surface orientation and a conforming contact interface. However, these pairs also exhibit the highest standard deviation and therefore the highest degree of uncertainty in predicting the heat transfer between contacting surfaces. In contrast, contact partners yielding a non-conforming interface, have significant lower standard deviation and but also smaller mean values. Concluding, this work offers a first approach to extend current contact heat transfer modeling with an additional parameter, considering the orientation of surface grooves and macroscopic structures. Future studies will include on the one hand more materials and more samples as well as evaluation with results predicted by numerical methods. On the other hand, the impact of surface structures on the thermal contact conductance for different magnitudes of microscopic surface roughness will be investigated.

Acknowledgement

The authors would like to thank the German research foundation (DFG) by founding the project collaborative research project TRR 96 Project-ID 174223256.

References

[1] R. Ramesh, M. Mannan, A. Poo, "Error compensation in machine tools - a review: Part ii: thermal errors," *International Journal of Machine Tools and Manufacture*, vol. 40, no. 9, pp. 1257-1284, 2000.

[2] J. Mayr, J. Jedrzejewski, E. Uhlmann, M. A. Donmez, W. Knapp, F. Haertig, K. Wendt, T. Moriwaki, P. Shore, R. Schmitt, et al., "Thermal issues in machine tools," *CIRP Annals-Manufacturing Technology*, vol. 61, no. 2, pp. 771-791, 2012.

[3] M. Cooper, B. Mikic, M. Yovanovich, "Thermal contact conductance," *International Journal of Heat and Mass Transfer*, vol. 12, no. 3, pp. 279-300, 1969.

[4] B. Mikic, "Thermal contact conductance; theoretical considerations," *International Journal of Heat and Mass Transfer*, vol. 17, no. 2, pp. 205-214, 1974.

[5] M. Yovanovich, "Thermal contact correlations," AIAA paper 81, pp. 83-95, 1982.

[6] M. Bahrami, M. Yovanovich, J. Culham, "Thermal joint resistances of conforming rough surfaces with gas."

[7] I. Savija, M. Yovanovich, J. Culham, E. Marotta, "Thermal joint resistance of conforming rough surfaces with grease-filled grease-filled interstitial gaps," *Journal of Thermophysics and Heat Transfer*, vol. 17, no. 2, pp. 278-282, 2003.

[8] M. M. Yovanovich, "Four decades of research on thermal contact, gap, and joint resistance in microelectronics," *IEEE Transactions on Components and Packaging Technologies*, vol. 28, no. 2, pp. 182-206, 2005.

[9] Y. Frekers, T. Helmig, E. Burghold, K. R, "A numerical approach for investigating thermal contact conductance," *International Journal of Thermal Sciences*, vol. 121, no. 2, pp. 45-54, 2017.

[10] I. Asiltürk H. Akkus, "Determining the effect cutting parameters on surface roughness in hard turning using the taguchi method," *Measurement*, vol. 44, no. 9, pp. 1697-1704, 2011.

[11] B. Bhushan, *Modern tribology handbook, two volume set*. CRC press, 2000.

[12] P. Benardos, G.-C. Vosniakos, "Predicting surface roughness in machining: a review," *International Journal of Machine Tools and Manufacture*, vol. 43, no. 8, pp. 833-844, 2003.

[13] O. Abouelatta, J. Madl, "Surface roughness prediction based on cutting parameters and tool vibrations inturning operations," *Journal of Materials Processing Technology*, vol. 118, no. 1-3, pp. 269-277, 2001.

[14] K. Risbood, U. Dixit, A. Sahasrabudhe, "Prediction of surface roughness and dimensional deviation by measuring cutting forces and vibrations in turning process," *Journal of Materials Processing Technology 360*, vol. 132, no. 1-3, pp. 203-214, 2003.

[15] E. Burghold, Y. Frekers, R. Kneer, “Transient contact heat transfer measurements based on high-speed IR-thermography,” *International Journal of Thermal Sciences*, vol. 115, pp. 169-175, 2017.
[16] E. Burghold, Y. Frekers, R. Kneer, “Determination of time-dependent thermal contact conductance through IR-thermography,” *International Journal of Thermal Sciences*, vol. 98, pp. 148-155, 2015.
[17] M. Deppermann, R. Kneer, “Determination of the heat flux to the workpiece during dry turning by inverse methods,” *Production Engineering*, vol. 9, no. 4, pp. 465-471, 2015.
[18] O. M. Alifanov, *Inverse heat transfer problems*. Springer Science & Business Media, 2012.
[19] M. N. Ozisik, *Inverse heat transfer: fundamentals and applications*. Routledge, 2018.
[20] J. Zhou, Y. Zhang, J. Chen, Z. Feng, “Inverse estimation of front surface temperature of a plate with laser heating and convection radiation cooling,” *International Journal of Thermal Sciences*, vol. 52, pp. 22-30, 2012.
[21] P. Duda, “A general method for solving transient multidimensional inverse heat transfer problems,” *International Journal of Heat and Mass Transfer*, vol. 93, pp. 665-673, 2016.